Composite failure prediction of π-joint structures under bending*

HUANG Hong-mei（黄红梅）**[1,2] and YUAN Shen-fang**（袁慎芳）**[1]****

1. Aeronautic Key Lab for Smart Materials and Structures, Nanjing University of Aeronautics and Astronautics, Nanjing 210016, China

2. College of Physics and Electronic Engineering, Xuzhou Normal University, Xuzhou 221116, China

In this article, the composite π-joint is investigated under bending loads. The "L" preform is the critical component regarding composite π-joint failure. The study is presented in the failure detection of a carbon fiber composite π-joint structure under bending loads using fiber Bragg grating (FBG) sensor. Firstly, based on the general finite element method (FEM) software, the 3-D finite element (FE) model of composite π-joint is established, and the failure process and every lamina failure load of composite π-joint are investigated by maximum stress criteria. Then, strain distributions along the length of FBG are extracted, and the reflection spectra of FBG are calculated according to the strain distribution. Finally, to verify the numerical results, a test scheme is performed and the experimental spectra of FBG are recorded. The experimental results indicate that the failure sequence and the corresponding critical loads of failure are consistent with the numerical predictions, and the computational error of failure load is less than 6.4%. Furthermore, it also verifies the feasibility of the damage detection system.

Adhesive composite joints nowadays play an important role in aerospace[1]. Accurate failure predictions are required for efficient joint design to utilize the advantages of adhesive bonding compared with mechanical fasteners[2-4], such as less weight of the total structure and lower assemble cost. The adhesive bonding joint, which is composed of two parts placed orthogonally and meeting at a joint, such as L-joint, T joint, and π-joint, is an effective way to use integrated composite structures. For example, American F-35 joint strike fighter used π-joints on the forward fuselage[3], and European EF-2000 fighter wing was used in the curing of skin and vertical web structure[4]. However, the joint is the weakness of the primary structure for the lack of reinforcement across the connected surfaces and through the occurrence of stress concentrations when it is subjected to load or transfers load applied on the structures. Thus, the failure prediction of the joint is very significant.

From all the possible adhesive joint designs, the π-joint is chosen for validation purposes in this study. The primary function of the joint is to transmit flexural, tensile and shear loads. In long time service, failures initiate due to operational load, aging, chemical attack, mechanical vibration and shocks[5,6]. So far, composite π-joint has been mostly analyzed on mechanical fasteners by Zhao Li-bin et al[7-9]. Existing techniques, such as X-ray, ultrasonic C-scan and laser shearography, have been applied to detect the damages[10]. However, it takes too much time to inspect the composite joint structures by these techniques. But the techniques can not realize online monitoring. Therefore, online monitoring of the damages in the composite joint structures is desired[11,12]. Fiber Bragg grating (FBG) sensor has been widely applied in the field of structural health monitoring for its light weight, small diameter, resistance to electromagnetic radiation, corrosion resistance and so on[13-15]. This paper studies a real-time online monitoring system using fiber Bragg grating sensor, which is used to monitor the failure of composite π-joint structure under bending loads.

We analyze the spectrum characteristics of FBG when it is under the uneven strain field. Here we assume a perturbation of the effective refractive index n_{eff} of the guided mode (s), which can be described by[16]

$$\delta n_{\text{eff}}(z) = \overline{\delta n_{\text{eff}}}(z)\left\{1+v\cos\left[\frac{2\pi}{\Lambda}z+\phi(z)\right]\right\}\ ,\qquad(1)$$

where $\overline{\delta n_{\text{eff}}}(z)$ is the "dc" index change spatially averaged over a grating period, v is the fringe visibility of the index change, Λ is the grating period, and $\phi(z)$ describes the grating chirp. In this paper, it means the chirp caused by a non-uniform strain field. If the factor is attributed to the period parameters, the refractive index modulation can be written as

$$\delta n_{\text{eff}}(z) = \overline{\delta n_{\text{eff}}}(z)\left\{1+v\cos\left[\frac{2\pi}{\Lambda(z)}z\right]\right\}\ ,\qquad(2)$$

where $\Lambda(z)$ is the effective period of FBG when it is subjected to a non-uniform strain. The effective period of FBG can be described by

$$\Lambda(z) = \Lambda_0[1+(1-pe)\varepsilon(z)]\ ,\qquad(3)$$

where Λ_0 is the nominal period of FBG, pe is the elasto-optical coefficient of optical fiber, and its value is equal to 0.26. From Eqs.(1), (2) and (3), the grating chirp $\phi(z)$ can be written as

$$\phi(z) = -\frac{2\pi z}{\Lambda_0}\left[\frac{(1-pe)\varepsilon(z)}{1+(1-pe)\varepsilon(z)}\right]\ .\qquad(4)$$

According to the weakly guiding condition and the coupled-mode theory, we can obtain the following simultaneous differential equations[17]

$$\frac{\mathrm{d}R}{\mathrm{d}z} = i\hat{\sigma}R(z)+i\kappa S(z)\ ,\qquad(5)$$

$$\frac{\mathrm{d}S}{\mathrm{d}z} = -i\hat{\sigma}S(z)-i\kappa R(z)\ ,\qquad(6)$$

where R and S are the amplitudes of the forward-propagating mode and the backward-propagating mode, respectively. $\hat{\sigma}$ is the general "dc" self-coupling coefficient, and κ is the "AC" coupling coefficient, which are defined as

$$\hat{\sigma} = \frac{2\pi}{\lambda}\overline{\delta n_{\text{eff}}}+2\pi n_{\text{eff}}\left(\frac{1}{\lambda}-\frac{1}{\lambda_D}\right)-\frac{1}{2}\frac{\mathrm{d}\phi}{\mathrm{d}z}\ ,\qquad(7)$$

$$\kappa = \frac{\pi}{\lambda}v\overline{\delta n_{\text{eff}}}\ .\qquad(8)$$

In Eq.(7), $\lambda_D = 2n_{\text{eff}}\Lambda_0$ is the designed wavelength which would be changed when FBG is subjected to various strain conditions. The reflection coefficient of FBG is defined as

$$\rho(z) = S(z)/R(z)\ .\qquad(9)$$

By substituting Eq.(9) into Eq.(5), we can obtain the following differential equation

$$\frac{\mathrm{d}\rho(z)}{\mathrm{d}z} = -i\kappa-2i\hat{\sigma}\rho(z)-ik\rho^2(z)\ .\qquad(10)$$

The length of the grating is assumed to be L (L=10 mm), so the limit of the grating is defined as $-L/2\leqslant z\leqslant L/2$, while the boundary conditions of FBG are $R(-L/2)=1$ and $S(L/2)=0$[17]. The researches used transmission matrix method to solve Eq.(10) before. In this paper, combining with Eqs.(4), (7) and (8), we solve it by Runge-Kutta method. Thus the reflectivity of grating $r=|\rho|^2$ can be obtained when the FBG is subjected to non-uniform strain.

In this paper, the composite π-joint consisting of a horizontal typical skin laminate, a vertical web, one "U" preform, one small horizontal preform and double "L" preforms, in which the vertical web is bonded to two corners and one horizontal preform, is investigated as shown in Fig.1. The material of composite π-joint is carbon fiber, and its properties are shown in Tab.1.
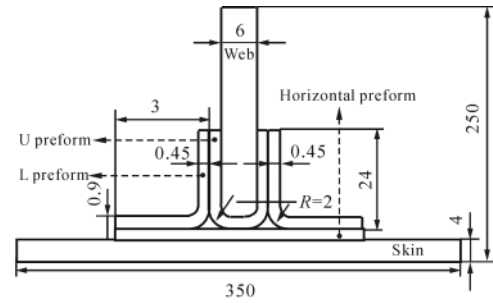

Fig.1 Schematic diagram and dimension parameters of the π-joint configuration (unit: mm)

Tab.1 Properties of material

Material	Angles of horizontal, "U" and "L" preforms	Material properties					
		E_1	$E_2=E_3$	$G_{12}=G_{13}$	G_{23}	$\mu_{12}=\mu_{13}$	μ_{23}
Carbon fiber	(-45°/0°/+45°)	135 GPa	8 GPa	4.5 GPa	3.7 GPa	0.3	0.35

In composite laminates, each lamina has two kinds of failure modes, which are matrix failure and fiber breakage. To the composite lamina in failure mode, two modified stiffness models, which are full stiffness elimination model and partial stiffness elimination model, are used in general. In the first method, as long as one lamina is in failure mode, regardless of its stiffness model, we assume that all stiffnesses of the lamina disappear, which means E_1=0, E_2=0 and G_{12}=0, but its thickness and location are not changed. In the second method, if the failure mode is matrix failure, we assume that the values of E_2 and G_{12} are equal to zero, but E_1 remains unchanged. If the failure mode is fiber breakage, the case is the same with the assumption in the first method[17]. In this paper, we can use the full stiffness elimination model.

It is shown in Refs.[7], [8] and [9] that "L" preform is the weakest part in the composite π-joint structure. Therefore, the

failure process of the "L" preform is studied under bending load. Firstly, determine its initial failure lamina and modifiy its stiffness, and then increase the load to find the second lamina. This process is repeated until all layers are faulted. Using this gradually failure analysis method, we can obtain the failure sequence of "L" preform and the corresponding critical load of each lamina. The calculation procedure is as following:

(1) Build the finite element (FE) model of π-joint; (2) Initial load is applied to the finite element model of π-joint, and then the node stress of each lamina is analyzed through the finite element software; (3) The node stresses are put into the Tsai-Wu criterion equation to make out the damage index of each lamina. Take the lamina, in which damage index is the biggest, as the lamina in failure mode, and then the critical load of failure is derived by maximum stress criterion; (4) According to the modified stiffness model, we can obtain the new stiffness of structure when one lamina is in failure mode; (5) Repeat steps 1 and 2 until all layers of the "L" preform are faulted.

Based on the FE analysis software ANSYS, for "U" preform, small horizontal preform and "L" preform, the FE models are set up with shell element, but for the other parts, the FE models are set up with solid element. Then, all parts are assembled to be a general structure. The FE model and FE mesh of the whole π-joint are given in Fig.2.

Fig.2 FE model and mesh of π-joint

The constraint conditions of π-joint should be decided by the experiment. The numerical analysis methodology encompasses the following basis assumption: (1) without considering the deformation, preload and friction force of the holding position; (2) the vertical displacements of the nodes on the holding position, in both forward and back sides of the skin, are constrained. In this stage, the model does not contain FBG sensor. Therefore, the failure sequence, the corresponding critical loads which are shown in Tab.2 and the strain distribution of the "L" preform can be obtained through the static analysis of the model, and also can be extracted from the analysis.

From the finite element method (FEM) analysis results, we can extract the strain distributions along the length of FBG, as shown in Fig.3. Thus, the reflection spectra of FBG

are calculated according to the strain distribution. During the calculation, the initial center wavelength of FBG is 1540 nm. The length (L), effective index (n_{eff}) and refractive index modulation ($\overline{\delta n_{eff}}$) of FBG are 10 mm, 1.45 and 0.0002, respectively.

Tab.2 Failure sequence and corresponding critical failure load of "L" preform

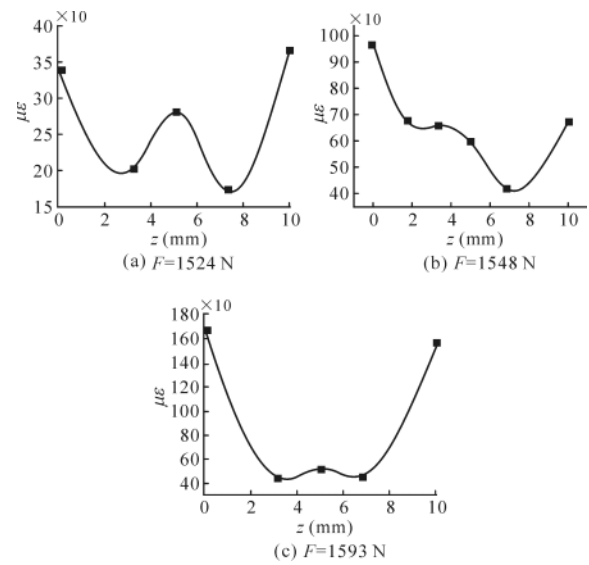| Failure sequence of "L" preform	1	2	3
Failure region	0° lamina	45° lamina	-45°lamina
Critical failure load	1524 N	1548 N	1593 N

Fig.3 Strain distribution along the FBG length corresponding to different failure laminas of "L" preform

Considering that the "L" preform is the weakest part of the composite π-joint structure, we arrange the FBG sensor between the "L" preform and the small horizontal preform. Testing of π-joint has been conducted at room temperature under a bending load. The experiment system is shown in Fig.4.
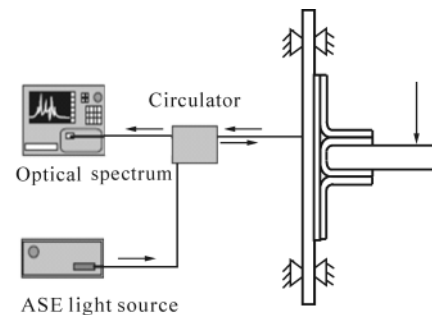

Fig.4 Schematic diagram of experiment system

The joint is subjected to bending load on the web, whose position is 50 mm away from the web top and clamped on the ends of skin. The FBG is illuminated by an amplified spontaneous emission (ASE) light source (AQ4130, Ando Electric Co., Ltd.), and the reflection spectra are obtained by

using an optical spectrum analyzer (AQ6317, Ando Electric Co., Ltd.). During the loading process, the spectra and corresponding loads are recorded when the spectrum changes and abnormal sound issues. The experimental results of two specimen are shown in Fig.5(b) and (c).
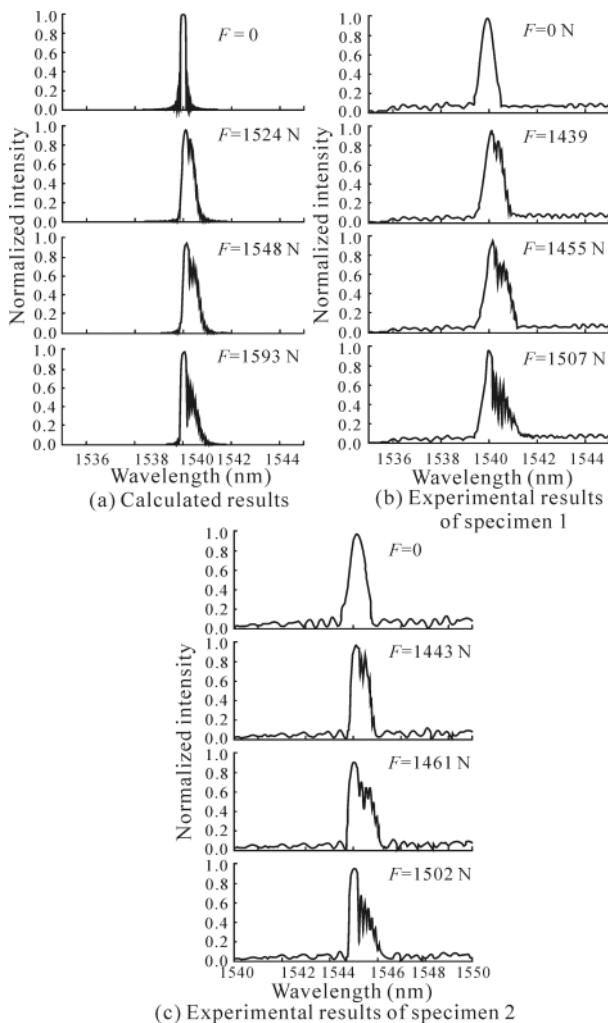

Fig.5 Reflection spectra of FBG

From Tab.2, we can obtain the failure process of the π-joint theoretically. The onset of failure occurs on the 0° lamina of L preform, next is the 45° lamina of L preform, and the ultimate failure occurs on the -45° lamina of L preform. The corresponding critical failure load is 1524 N, 1548 N and 1593 N, respectively. Experimental results are given in Fig.5 (b) and (c). The comparison of the results between calculation and experiment shows that they have good concordance. The error of failure critical loads is less than 6.4%, which is in the range of permitted errors in the field of structure health monitoring research. Besides, comparing the spectra in the different stages, though there is a slight difference between the measured and calculated spectra, the tendencies of the change in the spectra are consistent. Therefore, we can judge the failure sequence and the corresponding critical loads of "L" preform

in the π-joint structure by using the spectrum change of the FBG sensor.

The paper uses the carbon fiber π-joint structure as research object, and a real-time online monitoring system using FBG sensor is studied. The experimental results indicate that the failure sequence and the corresponding critical loads of failure are consistent with the numerical predictions, and the computational error of failure load is less than 6.4%. Furthermore, the feasibility of the damage detection system is verified, and it provides a foundation for the practical application of the FBG sensor in aerospace field.

References

[1] Du Shanyi, Acta Materiae Compositae Sinica **2**, 1 (2007).
[2] Shi Jian Zhong and Huang Yang, Acta Aeronautica Et Astronautica Sinica **7**, 493 (1998).
[3] Taylor R M and Owens S D, 45 th AIAA/ASME/ASCE/AHS/ASC Structures, Structural Dynamics & Materials Conference, Palm Springs, California, 2004.
[4] Yangnai Bin and Zhang Elaine, Composite Materials for Aircraft Structural Design, Beijing: Aviation Press, 2002.
[5] Sih GH and Skudra A M, Failure Mechanics of Composites, New York: Elsevier Science, 1985.
[6] Staszewski WJ, Boller C and Tomlinson GR, Health Monitoring of Aerospace Structures, Chichester: John Wiley & Sons, 2003.
[7] Zhao Libin, Peng Lei, Zhang Jianyu, Qin Mingliang, Liang Xianzhu, Chang Haifeng and Huang Hai, Acta Material Compositae Sinica **26**, 181(2009). (in Chinese)
[8] Zhao Libin, Dong Pei, Li jiaxi, HUANG Hai, LIANG Xianzhu and CAO Zhen-hua, Aeronautical Manufacturing Technology **21**, 61 (2007). (in Chinese)
[9] Zhao Libin, Qin Tianliang, Huang Hai, Li jiaxi, LIANG Xianzhu, CHANG Hai-feng and CAO Zhen-hua, Rare Materials and Engineering **38**, 105 (2009).
[10] Ruzek R, Lohonka R and Jironc J, Ultrasonic C-scan and Shearo-Graphy NDI Techniques of Impact Defects Identification, NDT and E International **39**, 132 (2006).
[11] Mickens T, Schulz M, Sundaresan M and Ghoshal A, Mech. Syst. Signal Proc. **17**, 285 (2003).
[12] Johnson TJ, Brown RL, Adams DE and Schiefer M, Mech. Syst. Sig Proc. **18**, 555 (2004).
[13] WANG Hong-liang, WANG Lin and JIA Zhen-an, Journal of Optoel- ectronics • Laser **20**, 526 (2009). (in Chinese)
[14] Mousumi Majumder, Tarun Kumar Gangopadhyay and Ashim Kumar Chakraborty, J. Sensors and Actuators A **147**, 150 (2008).
[15] HUANG Hong-mei and YUAN Shen-fang, Journal of Optoelectronics • Laser **22**, 109 (2011). (in Chinese)
[16] ZHAO Hai-tao, ZHANG Bo-ming and WU Zhan-jun, Journal of Optoelectronics • Laser **19**, 1172 (2008). (in Chinese)
[17] Chen JianQiao, Introduction to Mechanics of Composite Materials, Beijing: Science Press, 2006.